Human adherent cortical organoids in a multiwell format

Mark van der Kroeg[1], Sakshi Bansal[1], Maurits Unkel[1], Hilde Smeenk[1], Steven A. Kushner[1,3,4#*], Femke M.S. de Vrij[1,2#*]

[1]Department of Psychiatry, Erasmus MC, Rotterdam, 3015 CN, The Netherlands.

[2]ENCORE Expertise Center for Neurodevelopmental Disorders, Erasmus MC, Rotterdam, NL

[3]Dept. of Psychiatry, Columbia University Irving Medical Center, New York, NY, USA

[4]Stavros Niarchos Foundation (SNF) Center for Precision Psychiatry & Mental Health, Columbia University, New York, NY, USA

[#]These authors contributed equally

Contact information: *Correspondence: sk2602@cumc.columbia.edu, f.devrij@erasmusmc.nl.

Summary

In the growing diversity of human iPSC-derived models of brain development, we present here a novel method that exhibits 3D cortical layer formation in a highly reproducible topography of minimal dimensions. The resulting adherent cortical organoids develop by self-organization after seeding frontal cortex patterned iPSC-derived neural progenitor cells in 384-well plates during eight weeks of differentiation. The organoids have stereotypical dimensions of 3 x 3 x 0.2 mm, contain multiple subtypes of neurons, astrocytes and oligodendrocyte lineage cells, and are amenable to extended culture for at least 10 months. Longitudinal imaging revealed morphologically mature dendritic spines, axonal myelination, and robust neuronal activity. Moreover, adherent cortical organoids compare favorably to existing free-floating brain organoid models on the basis of robust reproducibility in obtaining topographically-standardized radial cortical structures and circumventing internal necrosis. Adherent human cortical organoids hold considerable potential for high-throughput drug discovery applications, neurotoxicological screening, and mechanistic pathophysiological studies of brain disorders.

Introduction

Human embryonic or induced pluripotent stem cell (hiPSC) derived models have yielded considerable success in elucidating neurodevelopmental biology in health and disease (Levy and Paşca, 2025). The approaches have been varied and complementary, including single cell hiPSC-derived models grown in a monolayer (Sarkar et al., 2018; Shan et al., 2024; Zhang et al., 2013), multiple neural cell types in 2D neural networks (Astick and Vanderhaeghen, 2018; Bardy et al., 2015; Gunhanlar et al., 2018; Shi et al., 2012), 3D free-floating regionalized neural organoids (Paşca et al., 2015; Qian et al., 2016a; Ullah et al., 2025; Xiang et al., 2019; Zhang et al., 2023), and hiPSC-derived free-floating unguided neural organoids and assembloids (Gomes et al., 2020; Kim et al., 2025; Lancaster et al., 2013; Paşca et al., 2025, 2022; Pellegrini et al., 2020; Renner et al., 2017; Sawada et al., 2020). Although models are continuing to improve, increasing cellular and topographical complexity has appeared to come at the cost of inter-organoid variability (Eichmüller and Knoblich, 2022; Kelava and Lancaster, 2016). Therefore, a major current technical challenge is to identify hiPSC-derived models that recapitulate higher-order neural complexity with reduced heterogeneity.

Existing 3D models suffer from considerable inter-organoid variability due to the complex and heterogeneous nature of the free-floating structures (Cederquist et al., 2019; He et al., 2024; Lancaster et al., 2013, 2017; Paşca et al., 2015; Renner et al., 2017; Velasco et al., 2019; Yoon et al., 2019). A further challenge, in particular with free-floating organoids, is the resulting necrotic core that frequently occurs when tissue volumes exceed the limits of oxygen and nutrient diffusion beyond a radius of ~300-400μm (Lancaster et al., 2017; Qian et al., 2016b; Uzquiano et al., 2022). Although recent progress has been made with slicing organoids prior to the emergence of necrosis, followed by organotypic air-liquid

interface culture (Giandomenico et al., 2019; Qian et al., 2020), even sliced organoids have to be repeatedly re-cut to prevent necrosis (Qian et al., 2020), which is both laborious and risks introducing another potential source of variability. The generation of vascularized organoids is currently a major focus in the field as a potential solution to reducing the necrotic core and some of the inherent cellular stress that is observed in cortical organoids. Moreover, xenotransplantation of organoids and hiPSC-derived neural cells into rodent brains also holds considerable promise as a model system to investigate circuit integration *in vivo* (Bhaduri et al., 2020; Fan et al., 2022; Pașca et al., 2025; Schafer et al., 2023; Vermaercke et al., 2024), but relies upon the use of animal models that limits advantages of a fully human cellular system. Increasing diffusion in organoids through microfluidics or vascularization (Kistemaker et al., 2025; Matsui et al., 2021) would be beneficial. Additionally, further investigation into the mutually supportive interactions between neural and vascular cells in a fully *in vitro* system composed exclusively of human cells is warranted (Crouch et al., 2022; Mansour et al., 2018; Wang et al., 2023) .

Here we propose a simplified approach to generating long-term hiPSC-derived adherent cortical organoids (ACO) with reproducible dimensions below metabolic diffusion limits in a readily screenable 384-well format. ACOs can be maintained in long-term culture and contain neurons with dendritic spines and robust activity, as well as several classes of glial cells including oligodendrocyte precursor cells (OPCs), myelinating oligodendrocytes, and morphologically distinct subtypes of astrocytes.

Results

Self-organized topography of iPSC-derived adherent cortical organoids

ACOs reproducibly self-organize into layered radial structures in 384-well plates within 8 weeks of seeding with hiPSC-derived purified forebrain-patterned neural progenitor cells (NPCs). Three different hiPSC source cell lines were used in this study, including commercially available NPCs, and NPCs generated using a modified version of our previously described protocol (Gunhanlar et al., 2018) (**Figure 1A**). NPCs were capable of neural rosette formation and expressed SOX2, Nestin, and the frontal cortical NPC-marker FOXG1 (**Figure 1B-D, Figure S1A).** The initial 4 weeks after seeding the NPCs in 384-well plates in Neural Differentiation Medium (ND) were characterized by proliferative expansion of NPCs and the emergence of early neural differentiation markers (**Figure 1E, Figure S2**). Between 4- and 8-weeks post-seeding, neurons and glial cells emerged with a consistent spatial organization (**Figure 1E, F, Figure S1B, Figure S2**), in which the central region was densely packed with cell bodies while the periphery contained circumferentially and radially organized processes originating from cells in the centre. Typically, ACOs with a single structure were observed in ~80% of the wells seeded with NPCs after 60 days of differentiation. Structural integrity remained quite stable and exhibited minimal decline over time with slight variation per cell line and per batch to an average of ~65% of wells with a single structure at day 234 and ~50% at day 310. (**Figure S1C**). Organoid topography was highly dependent on the proliferation rate of NPCs, which can differ substantially across differentiation batches and hiPSC clones. For each NPC line, optimal seeding density was estimated based on the proliferation rate of that NPC line. Multiple densities were seeded around the estimated optimal density, and after 6-8 weeks, the NPC density at which ACO generation were most reliably generated was determined empirically using a combination of visual inspection,

Live/Dead staining and immunocytochemistry. The proliferation rate and seeding density of NPCs required for generating topographically reliable ACOs were correlated (r^2=0.67) and provides guidance for empirically determining the optimal NPC seeding density for a given line (**Figure S1D**).

Cell type distribution and layer formation

Tau+/MAP2- axons exhibited long extensions in a circular pattern, while MAP2+ dendrites exhibited orthogonally oriented radial outgrowth (**Figure 2A, B Figure S3**). The spatial organisation that evolved over the first 8 weeks after seeding was paralleled by a shift in cell type distribution.

Overall, a reduction in progenitor markers (SOX2 day 14: 58.4%, day 56: 18.8% P = <0.001, PAX6 day 14: 34.5%, day 56: 8.0% P = 0.20) and a significant increase in neuronal cortical layer markers (CTIP2 day 14: 0.5%, day 56: 14.0% P = <0.001, CUX1 day 14: 1.3%, day 56: 24.4% P = <0.001) were observed (**Figure S2**). However, a SOX2 positive layer remained present in the centre of the ACOs at day 63 (**Figure S4C**). Cortical layer markers exhibited an inside-out pattern of development in which expression of the deep layer excitatory neuronal marker CTIP2 emerged before the upper layer marker CUX1 (**Figure S2**, **Figure 2C-E**). Six to eight weeks following seeding, a self-organised rudimentary segregation of deep- and upper layer neurons emerged as shown by the macroscopic separation of deep- and upper layer neurons, although some neurons were spatially intermixed and some neurons were double-positive for CTIP2 and CUX1. In the upper layer neuronal region, segregation was observed between CUX1 and CUX2 positive cells (**Figure 2E**) as CUX2 is typically expressed over a wider range of upper cortical layers than CUX1 and also marks intermediate progenitors (Molyneaux et al., 2007) (**Figure 2C, E, Figure S4**) Analogous to the

broad distribution of cortical cell subclasses, the majority of the neurons were glutamatergic, while GAD67+ interneurons were also present (**Figure 2F**), constituting ~10% of the NeuN+ neuronal population consistently for all three source hiPSC lines (**Figure 2G**) Over a developmental time course GAD67/NeuN remained relatively stable, although it showed a slight increase at differentiation day 114 (**Figure 2H**).

Adherent cortical organoids contain multiple glial cell types

Within 8 weeks of seeding, a population of GFAP+/S100β+ astrocytes emerged. Many astrocytes had their soma located in the central region with process outgrowth radially (**Figure 2I, Figure S5**), while other astrocytes exhibited subtype-specific morphologies including fibrous astrocytes (**Figure 2J**), protoplasmic-like astrocytes (**Figure 2K**) and interlaminar astrocytes (**Figure 2L**). GFAP/PAX6 double-positive radial glia were present at the outskirts of the densely populated centre of the organoid (**Figure 2M**).

Similar to free-floating organoids, ACOs survived for longer periods compared to monolayer neural cultures grown on larger surfaces. This longevity allows for the development of cell types not usually seen in a monolayer culture that can typically be cultured up to a maximum of 2 to 3 months. By 6 weeks after seeding NPCs, we observed the emergence of oligodendrocyte precursor cells (OPC), as shown by the expression of NG2 (**Figure 3A**) and the NG2+ cell population remained present when the first oligodendrocytes emerged (**Figure 3B/C**). Staining for Myelin Basic Protein (MBP) revealed the emergence of MBP+ oligodendrocytes around 4 months after NPC seeding when the ACOs were continuously grown in the presence of T3 (2ng/ml) (**Figure 3D**). At 5 months, the oligodendrocytes showed increasingly mature morphologies (**Figure 3E-I**) and exhibited MBP co-localization along NF200+ axons (**Figure 3F/I**).

Adherent cortical organoids show synaptic connectivity and functional activity

Neurons within ACOs exhibited robust synaptogenesis (**Figure 4A-E**). Sparse labelling of excitatory neurons with AAV9.CamKII.eGFP revealed the presence of Synapsin-positive (Syn+) mushroom-shaped dendritic spines (**Figure 4E**). 51.5% of the Syn+ presynaptic boutons co-localized with the excitatory post-synaptic density marker HOMER1 (**Figure 4F, I**), with a density of 10.9 Synapsin/HOMER1 double positive synapses per 100μm^2 MAP2 (**Figure 4H**). Moreover, 21.1% of Syn+ presynaptic boutons co-localized with the inhibitory post-synaptic density marker Gephyrin (**Figure 4G, H, I**), with a density of 5.0 Synapsin/Gephyrin double positive synapses per 100μm^2 MAP2. At differentiation day 114, we observed a ~2:1 ratio of excitatory to inhibitory synaptic contacts (**Figure 4H**).

To assess the functional activity of the ACOs, we used the genetically encoded calcium indicator GCaMP6s under the control of the human Synapsin promoter (**Figure 5A**). Calcium imaging revealed robust synchronous network-level bursting (NB) (1.4 $\pm$ 0.07 NB/min) at day 61 which remained stable until at least day 100 (1.6 $\pm$ 0.12 NB/min), in which all recorded neurons participated to varying degrees **(Figure 5B, D)**. In addition, substantial desynchronized activity was also observed outside of network-level bursting while the total activity remained stable over time (day 61, 3.9 $\pm$ 0.5 events/min; day 100, 3.9 $\pm$ 0.6 events/min) (**Figure 5B-E, Video 1**).

Discussion

The study of early human brain development and related diseases has long been hampered by the inherent complexity of the human brain and the inaccessibility of living brain tissue at cellular resolution. Technological advances in induced pluripotent stem cell technology have

now facilitated the opportunity to obtain living human neurons derived from specific individuals.

Here we describe a platform to model early human frontal cortical development with high reproducibility and simplified organization. While 3D free floating organoids and sliced organoids recapitulate layered cortex formation, they are subject to variation in the relative contribution of cortical tissue within the organoid, forming multiple cortical patches along the edges and complicating structured analysis (Eichmüller and Knoblich, 2022; Giandomenico et al., 2019; Quadrato et al., 2017). Moreover, 3D free floating organoids suffer from necrosis in the core of the organoid due to lack of oxygen and nutrient diffusion. Recently, other protocols have been published starting from rosette formation with a focus on early neurodevelopment and leading to single structure free floating cortical organoids (Pagliaro et al., 2023; Tidball et al., 2023). Our platform predefines a rosette-forming iPSC-derived cortical NPC population that self-organizes into adherent singular radial structures in a standard 384-well format. Other examples have highlighted the benefits of a multi-well format or systematic individual structure formation (Knight et al., 2018; Medda et al., 2016). Our platform now integrates these features to yield individual adherent layered cortical structures with synaptic connectivity and neuronal activity, as well as the major neural progenitor-derived glial cell types including OPCs, myelinating oligodendrocytes, and astrocytes. The reproducible format of adherent organoids in a 384-well format has the distinct advantage of being able to image entire organoids without slicing or clearing, including under live cell conditions. We confirmed the self-organizing potential and reproducibility of adherent cortical organoids across multiple hiPSC lines and using different sources of NPCs, controlling the seeding density for the proliferation rate of the specific NPC batch. Seeding NPCs with frontal cortical identity in the defined geometry of a 384-well plate

enabled the development of long-term functional neural networks in a complex radial structure resembling early human cortical development. Future studies aimed at single-cell RNA sequencing and advanced image-based analysis solutions in this platform will be important to further benchmark adherent organoids with topographical, typological and temporal hierarchies in the developing human cortex (Bhaduri et al., 2021; Nowakowski et al., 2017, 2016; Uzquiano et al., 2022). Functional ACOs in a multi-well format have the potential to be leveraged for high-throughput screening applications, neurotoxicological studies, mechanistic pathophysiological studies of neurodevelopmental and neuropsychiatric disorders, and pharmacological and phenotypic screening of disease phenotypes during early cortical development.

ACOs also have some limitations, most notably that cortical layering and regional specification appears to be more advanced in free-floating brain organoids, including gyrification in some models. Key characteristics of the model, including concurrent neuronal and astrocyte differentiation and a consistent ACO structure, were robust across hiPSC lines. Because oligodendrocytes arise later and require longer culture times, their generation showed greater variability. We are currently optimizing this aspect of the ACO model. Therefore, the choice of model system should be made based on the specific experimental question being addressed.

Taken together, we present a novel platform for cellular-level human brain modeling using adherent cortical organoids that exhibit high reproducibility and robust neuronal activity. The ability to reliably generate human cortical organoids in multi-well plates combined with neural network functionality offers a unique potential for brain disease modeling and therapeutic screening applications.

Materials and Methods

Generation of Neural Progenitor Cells

NPCs from 3 different source hiPSC lines were used. NPC-line 1: in house generated NPCs from human iPSC line WTC11 (Provided by Bruce R. Conklin, The Gladstone Institutes and UCSF, #GM25256, RRID:CVCL_Y803, Miyaoka et al.,2014). NPC-line 2: commercially available hNPCs from Axol Biosciences (ax0015). NPC-line 3: NPCs derived using the protocol of Shi et al., (Shi et al., 2012) from hiPSC line IPSC0028 (Sigma-Aldrich, RRID:CVCL_EE38). Line 1 NPCs were generated from the WTC11 hiPSC line grown on mouse embryonic fibroblasts (MEFs) in human embryonic stem cell medium (Dulbecco's modified Eagle's medium (DMEM)/F12 (Thermo Fisher Scientific), 20% knockout serum (Thermo Fisher Scientific), 1% minimum essential medium/non-essential amino acid (Sigma-Aldrich, St Louis, MO, USA), 7 nl ml β-mercaptoethanol (Sigma-Aldrich), 1% L-glutamine (Thermo Fisher Scientific) and 1% penicillin/streptomycin (Thermo Fisher Scientific). The hiPSC colonies were dissociated from the MEFs with collagenase (100 U ml, Thermo Fisher Scientific, Waltham, MA, USA) for 7 min at 37 °C/5% CO_2. Embryoid Bodies (EBs) were generated by transferring dissociated iPSCs to non-adherent plates in human embryonic stem cell medium on a shaker in at 37 °C/5% CO_2. EBs were grown for 2 days in human embryonic stem cell medium, changed into neural induction medium (Advanced DMEM/F12, 1% N2 supplement (Thermo Fisher Scientific), 2 µg ml heparin (Sigma-Aldrich) and 1% penicillin/streptomycin) on day 2 (d2) and cultured for another 5 days in suspension (d3–d7). The EBs were slightly dissociated at d7 by trituration and plated onto laminin-coated 10 cm dishes (20 µg ml laminin (Sigma-

Aldrich) in DMEM for 30 min at 37 °C), initially using neural induction medium (d7–d14), and then from d15 in NPC medium consisting of: Advanced DMEM/F12 (Life Technologies), 1% N2 supplement (Thermo Fisher Scientific), 2% B27-RA supplement (Thermo Fisher Scientific), 1 µg/ml laminin (L2020, Sigma-Aldrich), 20 ng/ml basic fibroblast growth factor (Merck-Millipore, Darmstadt, Germany) and 1% penicillin/streptomycin (Thermo Fisher Scientific). After passage 3, NPC cultures were purified using fluorescence-activated cell sorting (FACS). NPCs were detached from the culture plate using Accutase (Stem Cell Technologies) and $CD184^{+}/CD44^{-}/CD271^{-}/CD24^{+}$ cells (Yuan et al., 2011) were collected on a FACSAria III Cell Sorter (BD Bioscience) and expanded in NPC medium. NPCs were maintained in NPC medium on 6-well plates (Sanbio, 140675) coated with 20 µg/ml laminin (Sigma, L2020) in Advanced DMEM/F12 (Life Technologies) and were used for differentiation to adherent cortical organoids between passage 3 and 7 after the FACS purification step.

Generating Adherent Cortical Organoids

NPCs were dissociated with Accutase (Stem Cell Technologies), and live cells were counted with Trypan Blue (Stem Cell Technologies) in a Burker counting chamber. The NPCs were seeded in 384-well plates (M1937-32EA. Life Technologies) that were coated with 50 µg/ml laminin in Neurobasal medium (Thermo Fisher Scientific) for at least 30 minutes at 37 °C. The required seeding cell densities to generate ACOs for each individual cell line were determined by seeding a range of cell densities followed by visual inspection with a bright field microscope, Live/Dead staining and immunocytochemistry. When too few NPCs are seeded, the organoids will not form and show patches of clustered cells like you would see in a standard monolayer culture. When too many NPCs are seeded, the 384-plate well will

overgrow, leading to a lack of organoid structure formation. The variation in NPC seeding density is mostly explained by NPC proliferation rate, and to a lesser degree by the capacity of a given cell line to differentiate into post-mitotic neural cells. NPCs were seeded and differentiated in Neural Differentiation Medium: Neurobasal medium (Thermo Fisher Scientific), 1% N2 supplement (Thermo Fisher Scientific), 2% B27-RA supplement (Thermo Fisher Scientific), 1% minimum essential medium/non-essential amino acid (Stem Cell Technologies), 20 ng/ml brain-derived neurotrophic factor (ProSpec Bio), 20 ng/ml glial cell-derived neurotrophic factor (ProSpec Bio), 1 µM dibutyryl cyclic adenosine monophosphate (Sigma-Aldrich), 200 µM ascorbic acid (Sigma-Aldrich), 2 µg/ml laminin (Sigma-Aldrich) and 1% penicillin/streptomycin (Thermo Fisher Scientific). For oligodendrocyte maturation the cells were continuously grown in the presence of 2 ng/ml T3 (Sigma-Aldrich). Every 2-3 days the adherent cortical organoids were refreshed with a 75% media change.

Immunocytochemistry

For live-dead staining, living cultures were incubated with LIVE/DEAD™ Viability/Cytotoxicity Kit according to manufacturer's instructions (Thermo Fisher Scientific). For immunocytochemistry adherent cortical organoids were fixed for 20-30 minutes using 4% formaldehyde in phosphate-buffered saline (PBS), washed with PBS 3 times and blocked for 1 hour by pre-incubation in staining buffer containing 0.05 M Tris, 0.9% NaCl, 0.25% gelatin and 0.5% Triton-X-100 (pH 7.4). Primary antibodies were incubated for 48-72h at 4 °C in staining buffer, washed with PBS and incubated with the secondary antibodies in staining buffer for 2h at room temperature. The cultures were embedded in Mowiol 4-88 (Sigma-Aldrich), after which confocal imaging was performed with a Zeiss LSM700 and Zeiss

LSM800 confocal microscope using ZEN software (Zeiss, Oberkochen, Germany). The following primary antibodies were used: SOX2 (Merck-Millipore AB5603, 1:200); Nestin (Merck-Millipore MAB5326, 1:200); MAP2 (Synaptic Systems 188004, 1:200); NeuN (Merck ABN78, 1:200); GFAP (Merck-Millipore AB5804, 1:300); FOXG1 (Abcam AB18259, 1:200); CUX1 (Abcam AB54583, 1:200); CTIP2 (Abcam AB18465, 1:100); Synapsin 1/2 (Synaptic Systems 106003, 1:200); and PSD95 (Thermo Fisher Scientific MA1-046, 1:100); HOMER1 (Synaptic Systems 160011, 1:100) Gephyrin (Synaptic Systems 147011, 1:100); (Tau (Cell Signaling Technology 4019, 1:200); S100ß (Sigma-Aldrich S2532, 1:200); Pax6 (Santa Cruz sc-81649, 1:100); NG2 (Gift from W. Stallcup Lab, 1:100); NF200 (Sigma-Aldrich 083M4833, 1:200); MBP (Abcam AB7349, 1:100); GFP (Abcam ab13970, 1:100); GAD67 (Merck-Millipore MAB5406, 1:100) DAPI (Thermo Fisher Scientific D1306). The following secondary antibodies were used 1:200: Alexa-488, Alexa-555, Alexa-647 (Jackson ImmunoResearch, West Grove, PA, USA).

Sparse labelling of excitatory neurons

pENN.AAV9.CamKII.4.eGFP.WPRE.rBG (Addgene viral prep # 105541-AAV9) was added to the cortical organoids at day 278 ($1.68x10^8$ GC/well). The transduced cortical organoids were fixed and stained on day 310.

Synaptic Quantification

Following immunocytochemistry confocal imaging was performed with a Zeiss LSM800 confocal microscope with Airy scan using ZEN software (Zeiss, Oberkochen, Germany). Multiple images per organoid were taken of 157.94 µm by 157.94 µm with a depth of 10-15 µm with a scan every 0.17 µm. The surface area of MAP2 and the number of Synapsin+ pre-

synaptic terminals quantification was performed on a z-projection of the images in Fiji (Schindelin et al., 2012). The co-localization of Synapsin with either HOMER1 or Gephyrin was manually counted. The Day 114 data in Figure 4H and 4I was obtained from 4 organoids each with a total area of ~50000 μm^2 MAP2 and ~10000 Synapsin+ pre-synaptic terminals analysed.

Calcium imaging

For calcium imaging, the genetically encoded calcium indicator AAV1.Syn.GCaMP6s.WPRE.SV40 (Penn Vector Core, 100843-AAV1) was added to the organoids at day 42 of differentiation ($1.5x10^8$ GC/well). Recordings were performed at day 60 on a Zeiss LSM800 confocal microscope using ZEN software (Zeiss, Oberkochen, Germany). The recordings were made with a 20x/0.8NA Ph2 Plan-Apochromat objective, with a field of view of 150 × 100 µm and a pixel size of 0,3 µm. The acquisition rates of the recordings were between 4-5 f.p.s. 24 hours before the recordings, the medium was switched to BrainPhys Neural Differentiation Medium. BrainPhys Neuronal Media (Stem Cell Technologies), 1% N2 supplement (Thermo Fisher Scientific), 2% B27-RA supplement (Thermo Fisher Scientific), 1% minimum essential medium/non-essential amino acid (Stem Cell Technologies), 1% penicillin/streptomycin (Thermo Fisher Scientific), 20 ng/ml brain-derived neurotrophic factor (ProSpec Bio), 20 ng/ml glial cell-derived neurotrophic factor (ProSpec Bio), 1 µM dibutyryl cyclic adenosine monophosphate (Sigma-Aldrich), 200 µM ascorbic acid (Sigma-Aldrich) and 2 µg/ml laminin (Sigma-Aldrich). The calcium imaging recordings were processed using CNMF-E (Pnevmatikakis et al., 2016) and FluoroSNAPP (Patel et al., 2015) to generate the traces. Calcium traces were then analysed using a custom script for event and network burst detection using an algorithm written in

Python (v3.8.2) (code accessibility can be requested via Github). A network burst is defined here as synchronous calcium events of at least 60% of the active neurons in the field of view.

Cyquant Proliferation Assay

CyQUANT™ Direct Cell Proliferation Assay, C35011 (Thermo Fisher Scientific) was used according to manufacturer specifications. For each time point and each of the 3 NPC lines 10-12 wells of a 96-well plate were seeded with NPCs (2500 NPCs per well). In addition, NPC lines generated from 2 different clones from IPS line MH0159020 (Rutgers University Cell and DNA Repository) were added to increase the dynamic range of the proliferation curve. At 24h and 96h NPCs were frozen at -80°C. All NPC lines and timepoints were thawed, lysed and measured together. Doubling time was calculated between 24h and 96h. None of the wells were confluent at 96h.

Statistical analysis

All data represent mean ± SEM. When comparing developmental markers in Figure S2 we used one-way ANOVA followed by Tukey- Kramer's multiple correction test. n=3-6 images taken over two wells, for each time point. To compare the time points in Figure 5C-E we used a Mann-Whitney test.

Acknowledgements

This work was supported by the Netherlands Organ-on-Chip Initiative, an NWO Gravitation project funded by the Ministry of Education, Culture and Science of the government of the Netherlands (024.003.001) to SAK, Hersenstichting Fellowship (F2012(1)-39) to FMSdV, an

Erasmus MC Human Disease Model Award to FMSdV and a Dutch ZonMw MKMD Create2Solve grant (114025201) to SAK and FMSdV.

Author contributions

MvdK, SB and HS performed experiments, MU developed calcium imaging analysis algorithms, FdV and SAK supervised the work, MvdK, FdV and SAK wrote the paper.

Declaration of interests

The authors declare no competing interests.

References

Astick M, Vanderhaeghen P. 2018. From Human Pluripotent Stem Cells to Cortical Circuits. *Curr Top Dev Biol* **129**:67–98. doi:10.1016/bs.ctdb.2018.02.011

Bardy C, van den Hurk M, Eames T, Marchand C, Hernandez R V, Kellogg M, Gorris M, Galet B, Palomares V, Brown J, Bang AG, Mertens J, Böhnke L, Boyer L, Simon S, Gage FH. 2015. Neuronal medium that supports basic synaptic functions and activity of human neurons in vitro. *Proc Natl Acad Sci U S A* **112**. doi:10.1073/pnas.1504393112

Bhaduri A, Andrews MG, Mancia Leon W, Jung DD, Shin D, Allen D, Jung DD, Schmunk G, Haeussler M, Salma J, Pollen AA, Nowakowski TJ, Kriegstein AR. 2020. Cell stress in cortical organoids impairs molecular subtype specification. *Nature* 1–7. doi:10.1038/s41586-020-1962-0

Bhaduri A, Sandoval-Espinosa C, Otero-Garcia M, Oh I, Yin R, Eze UC, Nowakowski TJ, Kriegstein AR. 2021. An atlas of cortical arealization identifies dynamic molecular signatures. *Nature* **598**:200–204. doi:10.1038/s41586-021-03910-8

Cederquist GY, Asciolla JJ, Tchieu J, Walsh RM, Cornacchia D, Resh MD, Studer L. 2019. Specification of positional identity in forebrain organoids. *Nat Biotechnol* **37**:436–444. doi:10.1038/s41587-019-0085-3

Crouch EE, Bhaduri A, Andrews MG, Cebrian-Silla A, Diafos LN, Birrueta JO, Wedderburn-Pugh K, Valenzuela EJ, Bennett NK, Eze UC, Sandoval-Espinosa C, Chen J, Mora C, Ross JM, Howard CE, Gonzalez-Granero S, Lozano JF, Vento M, Haeussler M, Paredes MF, Nakamura K, Garcia-Verdugo JM, Alvarez-Buylla A, Kriegstein AR, Huang EJ. 2022. Ensembles of endothelial and mural cells promote angiogenesis in prenatal human brain. *Cell* **185**:3753-3769.e18. doi:10.1016/j.cell.2022.09.004

Eichmüller OL, Knoblich JA. 2022. Human cerebral organoids — a new tool for clinical neurology research. *Nat Rev Neurol* **18**:661–680. doi:10.1038/s41582-022-00723-9

Fan W, Christian KM, Song H, Ming G li. 2022. Applications of Brain Organoids for Infectious Diseases. *J Mol Biol* **434**:167243. doi:10.1016/j.jmb.2021.167243

Giandomenico SL, Mierau SB, Gibbons GM, Wenger LMD, Masullo L, Sit T, Sutcliffe M, Boulanger J, Tripodi M, Derivery E, Paulsen O, Lakatos A, Lancaster MA. 2019. Cerebral organoids at the air–liquid interface generate diverse nerve tracts with functional output. *Nat Neurosci* **22**:669–679. doi:10.1038/s41593-019-0350-2

Gomes AR, Fernandes TG, Vaz SH, Silva TP, Bekman EP, Xapelli S, Duarte S, Ghazvini M, Gribnau J, Muotri AR, Trujillo CA, Sebastião AM, Cabral JMS, Diogo MM. 2020. Modeling Rett Syndrome With Human Patient-Specific Forebrain Organoids. *Front Cell Dev Biol* **8**:1–18. doi:10.3389/fcell.2020.610427

Gunhanlar N, Shpak G, van der Kroeg M, Gouty-Colomer LA, Munshi ST, Lendemeijer B, Ghazvini M, Dupont C, Hoogendijk WJG, Gribnau J, de Vrij FMS, Kushner SA. 2018. A simplified protocol for differentiation of electrophysiologically mature neuronal

networks from human induced pluripotent stem cells. *Mol Psychiatry* **23**:1336–1344. doi:10.1038/mp.2017.56

He Z, Dony L, Fleck JS, Szałata A, Li KX, Slišković I, Lin HC, Santel M, Atamian A, Quadrato G, Sun J, Pașca SP, Binder EB, Cruceanu C, Testa G, Villa E, Caporale N, Bowles KR, Temple S, Bertucci T, Kelley KW, Amin ND, Camp JG, Theis FJ, Treutlein B. 2024. An integrated transcriptomic cell atlas of human neural organoids. *Nature* **635**:690–698. doi:10.1038/s41586-024-08172-8

Kelava I, Lancaster MAA. 2016. Stem Cell Models of Human Brain Development. *Cell Stem Cell* **18**:736–748. doi:10.1016/j.stem.2016.05.022

Kim J Il, Imaizumi K, Jurjuț O, Kelley KW, Wang D, Thete MV, Hudacova Z, Amin ND, Levy RJ, Scherrer G, Pașca SP. 2025. Human assembloid model of the ascending neural sensory pathway. *Nature* **642**:143–153. doi:10.1038/s41586-025-08808-3

Kistemaker L, van Bodegraven EJ, de Vries HE, Hol EM. 2025. Vascularized human brain organoids: current possibilities and prospects. *Trends Biotechnol* **43**:1275–1285. doi:10.1016/j.tibtech.2024.11.021

Knight GT, Lundin BF, Iyer N, Ashton LMT, Sethares WA, Willett RM, Ashton RS. 2018. Engineering induction of singular neural rosette emergence within hPSC-derived tissues. *Elife* **7**. doi:10.7554/eLife.37549

Lancaster M a, Renner M, Martin C-A, Wenzel D, Bicknell LS, Hurles ME, Homfray T, Penninger JM, Jackson AP, Knoblich JA. 2013. Cerebral organoids model human brain development and microcephaly. *Nature* **501**:373–379. doi:10.1038/nature12517

Lancaster MA, Corsini NS, Wolfinger S, Gustafson EH, Phillips AW, Burkard TR, Otani T, Livesey FJ, Knoblich JA. 2017. Guided self-organization and cortical plate formation in human brain organoids. *Nat Biotechnol* **35**:659–666. doi:10.1038/nbt.3906

Levy RJ, Paşca SP. 2025. From Organoids to Assembloids: Experimental Approaches to Study Human Neuropsychiatric Disorders. *Annu Rev Neurosci*. doi:10.1146/ANNUREV-NEURO-112723-023232

Mansour AA, Gonçalves JT, Bloyd CW, Li H, Fernandes S, Quang D, Johnston S, Parylak SL, Jin X, Gage FH. 2018. An in vivo model of functional and vascularized human brain organoids. *Nat Biotechnol* **36**:432–441. doi:10.1038/nbt.4127

Matsui TK, Tsuru Y, Hasegawa K, Kuwako K ichiro. 2021. Vascularization of human brain organoids. *Stem Cells* **39**:1017–1024. doi:10.1002/stem.3368

Medda X, Mertens L, Versweyveld S, Diels A, Barnham L, Bretteville A, Buist A, Verheyen A, Royaux I, Ebneth A, Cabrera-Socorro A. 2016. Development of a Scalable, High-Throughput-Compatible Assay to Detect Tau Aggregates Using iPSC-Derived Cortical Neurons Maintained in a Three-Dimensional Culture Format. *J Biomol Screen*. doi:10.1177/1087057116638029

Molyneaux BJ, Arlotta P, Menezes JRL, Macklis JD. 2007. Neuronal subtype specification in the cerebral cortex. *Nat Rev Neurosci* **8**:427–37. doi:10.1038/nrn2151

Nowakowski TJ, Bhaduri A, Pollen AA, Alvarado B, Mostajo-Radji MA, Di Lullo E, Haeussler M, Sandoval-Espinosa C, Liu SJ, Velmeshev D, Ounadjela JR, Shuga J, Wang X, Lim DA, West JA, Leyrat AA, Kent WJ, Kriegstein AR. 2017. Spatiotemporal gene expression trajectories reveal developmental hierarchies of the human cortex. *Science (80-)* **358**. doi:10.1126/science.aap8809

Nowakowski TJ, Pollen AA, Sandoval-Espinosa C, Kriegstein AR. 2016. Transformation of the Radial Glia Scaffold Demarcates Two Stages of Human Cerebral Cortex Development. *Neuron* **91**. doi:10.1016/j.neuron.2016.09.005

Pagliaro A, Finger R, Zoutendijk I, Bunschuh S, Clevers H, Hendriks D, Artegiani B. 2023.

Temporal morphogen gradient-driven neural induction shapes single expanded neuroepithelium brain organoids with enhanced cortical identity. *Nat Commun* **14**. doi:10.1038/s41467-023-43141-1

Paşca AM, Sloan SA, Clarke LE, Tian Y, Makinson CD, Huber N, Kim CH, Park J-Y, O'Rourke NA, Nguyen KD, Smith SJ, Huguenard JR, Geschwind DH, Barres BA, Paşca SP. 2015. Functional cortical neurons and astrocytes from human pluripotent stem cells in 3D culture. *Nat Methods*. doi:10.1038/nmeth.3415

Paşca SP, Arlotta P, Bateup HS, Camp JG, Cappello S, Gage FH, Knoblich JA, Kriegstein AR, Lancaster MA, Ming G-L, Muotri AR, Park I-H, Reiner O, Song H, Studer L, Temple S, Testa G, Treutlein B, Vaccarino FM. 2022. A nomenclature consensus for nervous system organoids and assembloids. *Nat 2022 6097929* **609**:907–910. doi:10.1038/s41586-022-05219-6

Paşca SP, Arlotta P, Bateup HS, Camp JG, Cappello S, Gage FH, Knoblich JA, Kriegstein AR, Lancaster MA, Ming GL, Novarino G, Okano H, Parmar M, Park IH, Reiner O, Song H, Studer L, Takahashi J, Temple S, Testa G, Treutlein B, Vaccarino FM, Vanderhaeghen P, Young-Pearse T. 2025. A framework for neural organoids, assembloids and transplantation studies. *Nature* **639**:315–320. doi:10.1038/s41586-024-08487-6

Patel TP, Man K, Firestein BL, Meaney DF. 2015. Automated quantification of neuronal networks and single-cell calcium dynamics using calcium imaging. *J Neurosci Methods* **243**:1–13. doi:10.1016/j.jneumeth.2015.01.020

Pellegrini L, Bonfio C, Chadwick J, Begum F, Skehel M, Lancaster MA. 2020. Human CNS barrier-forming organoids with cerebrospinal fluid production. *Science (80-)* **369**. doi:10.1126/science.aaz5626

Qian X, Nguyen HN, Song MM, Hadiono C, Ogden SC, Hammack C, Yao B, Hamersky GR,

Jacob F, Zhong C, Yoon KJ, Jeang W, Lin L, Li Y, Thakor J, Berg DA, Zhang C, Kang E, Chickering M, Nauen D, Ho CY, Wen Z, Christian KM, Shi PY, Maher BJ, Wu H, Jin P, Tang H, Song H, Ming GL. 2016b. Brain-Region-Specific Organoids Using Mini-bioreactors for Modeling ZIKV Exposure. *Cell* **165**:1238–1254. doi:10.1016/j.cell.2016.04.032

Qian X, Su Y, Adam CD, Deutschmann AU, Pather SR, Goldberg EM, Su K, Li S, Lu L, Jacob F, Nguyen PTT, Huh S, Hoke A, Swinford-Jackson SE, Wen Z, Gu X, Pierce RC, Wu H, Briand LA, Chen HI, Wolf JA, Song H, Ming G. 2020. Sliced Human Cortical Organoids for Modeling Distinct Cortical Layer Formation. *Cell Stem Cell* **26**:766-781.e9. doi:10.1016/j.stem.2020.02.002

Qian Xuyu, Nguyen Ha Nam, Song MM, Hadiono C, Ogden Sarah C., Hammack Christy, Yao Bing, Hamersky GR, Jacob F, Zhong C, Yoon K, Jeang W, Lin L, Li Yujing, Thakor J, Berg DA, Zhang Ce, Kang E, Chickering M, Nauen David, Ho C-Y, Wen Zhexing, Christian KM, Shi P-Y, Maher Brady J., Wu H, Jin P, Tang Hengli, Song H, Ming G, Bayer A, Lennemann NJ, Ouyang Y, Bramley JC, Morosky S, Marques ETJ, Cherry S, Sadovsky Y, Coyne CB, Ben-Ari Y, Spitzer NC, Blackshaw S, Scholpp S, Placzek M, Ingraham H, Simerly R, Shimogori T, Calvet G, Aguiar RS, Melo AS, Sampaio SA, Filippis I de, Fabri A, Araujo ES, Sequeira PC de, Mendonça MC de, Oliveira L de, al. et, Cauchemez S, Besnard M, Bompard P, Dub T, Guillemette-Artur P, Eyrolle-Guignot D, Salje H, Kerkhove MD Van, Abadie V, Garel C, al. et, Chung S, Hedlund E, Hwang M, Kim DW, Shin BS, Hwang DY, Kang UJ, Isacson O, Kim KS, Danjo T, Eiraku M, Muguruma K, Watanabe K, Kawada M, Yanagawa Y, Rubenstein JL, Sasai Y, Driggers RW, Ho CY, Korhonen EM, Kuivanen S, Jääskeläinen AJ, Smura T, Rosenberg A, Hill DA, DeBiasi RL, Vezina G, al. et, Faria NR, Azevedo RD, Kraemer MU, Souza R, Cunha MS, Hill SC, Thézé J, Bonsall MB, Bowden

TA, Rissanen I, al. et, Garcez PP, Loiola EC, Costa RM da, Higa LM, Trindade P, Delvecchio R, Nascimento JM, Brindeiro R, Tanuri A, Rehen SK, Goodwin TJ, Schroeder WF, Wolf DA, Moyer MP, Haddow AD, Schuh AJ, Yasuda CY, Kasper MR, Heang V, Huy R, Guzman H, Tesh RB, Weaver SC, Hansen DV, Lui JH, Parker PR, Kriegstein AR, Heymann DL, Hodgson A, Sall AA, Freedman DO, Staples JE, Althabe F, Baruah K, Mahmud G, Kandun N, Vasconcelos PF, al. et, Jaffe AE, Shin J, Collado-Torres L, Leek JT, Tao R, Li C, Gao Y, Jia Y, Maher B.J., Hyde TM, al. et, Jessup JM, Goodwin TJ, Spaulding G, Kadoshima T, Sakaguchi H, Nakano T, Soen M, Ando S, Eiraku M, Sasai Y, Kim JY, Liu CY, Zhang F, Duan X, Wen Z., Song J, Feighery E, Lu B, Rujescu D, Clair DS, al. et, Kriks S, Shim JW, Piao J, Ganat YM, Wakeman DR, Xie Z, Carrillo-Reid L, Auyeung G, Antonacci C, Buch A, al. et, Kundakovic M, Gudsnuk K, Franks B, Madrid J, Miller RL, Perera FP, Champagne FA, Lancaster MA, Knoblich JA, Lancaster MA, Renner M, Martin CA, Wenzel D, Bicknell LS, Hurles ME, Homfray T, Penninger JM, Jackson AP, Knoblich JA, Lazear HM, Govero J, Smith AM, Platt DJ, Fernandez E, Miner JJ, Diamond MS, Lui JH, Hansen DV, Kriegstein AR, Mariani J, Coppola G, Zhang P, Abyzov A, Provini L, Tomasini L, Amenduni M, Szekely A, Palejev D, Wilson M, al. et, Mlakar J, Korva M, Tul N, Popović M, Poljšak-Prijatelj M, Mraz J, Kolenc M, Rus KR, Vipotnik TV, Vodušek VF, al. et, Muguruma K, Nishiyama A, Kawakami H, Hashimoto K, Sasai Y, Paşca AM, Sloan SA, Clarke LE, Tian Y, Makinson CD, Huber N, Kim CH, Park JY, O'Rourke NA, Nguyen KD, al. et, Petanjek Z, Berger B, Esclapez M, Pollen AA, Nowakowski TJ, Chen J, Retallack H, Sandoval-Espinosa C, Nicholas CR, Shuga J, Liu SJ, Oldham MC, Diaz A, al. et, Roost MS, Iperen L van, Ariyurek Y, Buermans HP, Arindrarto W, Devalla HD, Passier R, Mummery CL, Carlotti F, Koning EJ de, al. et, Tang H., Hammack C., Ogden S.C., Wen Z., Qian X., Li Y., Yao B., Shin J, Zhang F, Lee EM, al. et, Thomsen ER, Mich JK, Yao Z, Hodge RD, Doyle

AM, Jang S, Shehata SI, Nelson AM, Shapovalova NV, Levi BP, al. et, Wang W, Lufkin T, Wen Z., Nguyen H.N., Guo Z, Lalli MA, Wang X, Su Y, Kim NS, Yoon KJ, Shin J, Zhang C., al. et, Yin X, Mead BE, Safaee H, Langer R, Karp JM, Levy O, Yoon KJ, Nguyen H.N., Ursini G, Zhang F, Kim NS, Wen Z., Makri G, Nauen D., Shin JH, Park Y, al. et, Yu X, Zecevic N. 2016a. Brain-Region-Specific Organoids Using Mini-bioreactors for Modeling ZIKV Exposure. *Cell* **165**:1238–1254. doi:10.1016/j.cell.2016.04.032

Quadrato G, Nguyen T, Macosko EZ, Sherwood JL, Min Yang S, Berger DR, Maria N, Scholvin J, Goldman M, Kinney JP, Boyden ES, Lichtman JW, Williams ZM, McCarroll SA, Arlotta P. 2017. Cell diversity and network dynamics in photosensitive human brain organoids. *Nature* **545**:48–53. doi:10.1038/nature22047

Renner M, Lancaster MA, Bian S, Choi H, Ku T, Peer A, Chung K, Knoblich JA. 2017. Self-organized developmental patterning and differentiation in cerebral organoids. *EMBO J* **36**:1316–1329. doi:10.15252/embj.201694700

Sarkar A, Mei A, Paquola ACM, Stern S, Bardy C, Klug JR, Kim S, Neshat N, Kim HJ, Ku M, Shokhirev MN, Adamowicz DH, Marchetto MC, Jappelli R, Erwin JA, Padmanabhan K, Shtrahman M, Jin X, Gage FH. 2018. Efficient Generation of CA3 Neurons from Human Pluripotent Stem Cells Enables Modeling of Hippocampal Connectivity In Vitro. *Cell Stem Cell* **22**:684-697.e9. doi:10.1016/j.stem.2018.04.009

Sawada T, Chater TE, Sasagawa Y, Yoshimura M, Fujimori-Tonou N, Tanaka K, Benjamin KJM, Paquola ACM, Erwin JA, Goda Y, Nikaido I, Kato T. 2020. Developmental excitation-inhibition imbalance underlying psychoses revealed by single-cell analyses of discordant twins-derived cerebral organoids. *Mol Psychiatry* **25**:2695–2711. doi:10.1038/s41380-020-0844-z

Schafer ST, Mansour AAF, Schlachetzki JCM, Pena M, Ghassemzadeh S, Mitchell L, Mar A,

Quang D, Stumpf S, Ortiz IS, Lana AJ, Baek C, Zaghal R, Glass CK, Nimmerjahn A, Gage FH. 2023. An in vivo neuroimmune organoid model to study human microglia phenotypes. *Cell* **186**:2111-2126.e20. doi:10.1016/j.cell.2023.04.022

Schindelin J, Arganda-Carreras I, Frise E, Kaynig V, Longair M, Pietzsch T, Preibisch S, Rueden C, Saalfeld S, Schmid B, Tinevez JY, White DJ, Hartenstein V, Eliceiri K, Tomancak P, Cardona A. 2012. Fiji: An open-source platform for biological-image analysis. *Nat Methods* **9**:676–682. doi:10.1038/nmeth.2019

Shan X, Zhang A, Rezzonico MG, Tsai MC, Sanchez-Priego C, Zhang Y, Chen MB, Choi M, Andrade López JM, Phu L, Cramer AL, Zhang Q, Pattison JM, Rose CM, Hoogenraad CC, Jeong CG. 2024. Fully defined NGN2 neuron protocol reveals diverse signatures of neuronal maturation. *Cell Reports Methods* **4**. doi:10.1016/j.crmeth.2024.100858

Shi Y, Kirwan P, Smith J, Robinson HPC, Livesey FJ. 2012. Human cerebral cortex development from pluripotent stem cells to functional excitatory synapses. *Nat Neurosci* **15**:477–86, S1. doi:10.1038/nn.3041

Tidball AM, Niu W, Ma Q, Takla TN, Walker JC, Margolis JL, Mojica-Perez SP, Sudyk R, Deng L, Moore SJ, Chopra R, Shakkottai VG, Murphy GG, Yuan Y, Isom LL, Li JZ, Parent JM. 2023. Deriving early single-rosette brain organoids from human pluripotent stem cells. *Stem Cell Reports* **18**:2498–2514. doi:10.1016/j.stemcr.2023.10.020

Ullah HMA, Huang Q, Chiola S, Wang Y, Shcheglovitov A. 2025. Generating and characterizing human telencephalic brain organoids from stem cell-derived single neural rosettes. *Nat Protoc*. doi:10.1038/s41596-025-01197-x

Uzquiano A, Kedaigle AJ, Pigoni M, Paulsen B, Adiconis X, Kim K, Faits T, Nagaraja S, Antón-Bolaños N, Gerhardinger C, Tucewicz A, Murray E, Jin X, Buenrostro J, Chen F, Velasco S, Regev A, Levin JZ, Arlotta P. 2022. Proper acquisition of cell class identity in

organoids allows definition of fate specification programs of the human cerebral cortex. *Cell* **185**:3770-3788.e27. doi:10.1016/j.cell.2022.09.010

Velasco S, Kedaigle AJ, Simmons SK, Nash A, Rocha M, Quadrato G, Paulsen B, Nguyen L, Adiconis X, Regev A, Levin JZ, Arlotta P. 2019. Individual brain organoids reproducibly form cell diversity of the human cerebral cortex. *Nature* 1. doi:10.1038/s41586-019-1289-x

Vermaercke B, Iwata R, Wierda K, Boubakar L, Rodriguez P, Ditkowska M, Bonin V, Vanderhaeghen P. 2024. SYNGAP1 deficiency disrupts synaptic neoteny in xenotransplanted human cortical neurons in vivo. *Neuron* **112**:3058-3068.e8. doi:10.1016/j.neuron.2024.07.007

Wang M, Gage FH, Schafer ST. 2023. Transplantation Strategies to Enhance Maturity and Cellular Complexity in Brain Organoids. *Biol Psychiatry* **93**:616–621. doi:10.1016/j.biopsych.2023.01.004

Xiang Y, Tanaka Y, Cakir B, Patterson B, Kim K-Y, Sun P, Kang Y-J, Zhong M, Liu X, Patra P, Lee S-H, Weissman SM, Park I-H. 2019. hESC-Derived Thalamic Organoids Form Reciprocal Projections When Fused with Cortical Organoids. *Cell Stem Cell* **24**:487-497.e7. doi:10.1016/J.STEM.2018.12.015

Yoon S-J, Elahi LS, Pașca AM, Marton RM, Gordon A, Revah O, Miura Y, Walczak EM, Holdgate GM, Fan HC, Huguenard JR, Geschwind DH, Pașca SP. 2019. Reliability of human cortical organoid generation. *Nat Methods* **16**:75–78. doi:10.1038/s41592-018-0255-0

Yuan SH, Martin J, Elia J, Flippin J, Paramban RI, Hefferan MP, Vidal JG, Mu Y, Killian RL, Israel MA, Emre N, Marsala S, Marsala M, Gage FH, Goldstein LSB, Carson CT. 2011. Cell-Surface Marker Signatures for the Isolation of Neural Stem Cells, Glia and Neurons

Derived from Human Pluripotent Stem Cells. *PLoS One* **6**:e17540. doi:10.1371/journal.pone.0017540

Zhang Y, Pak C, Han Y, Ahlenius H, Zhang Z, Chanda S, Marro S, Patzke C, Acuna C, Covy J, Xu W, Yang N, Danko T, Chen L, Wernig M, Südhof TCCC. 2013. Rapid Single-Step Induction of Functional Neurons from Human Pluripotent Stem Cells. *Neuron* **78**:785–798. doi:10.1016/j.neuron.2013.05.029

Zhang Z, Wang X, Park S, Song H, Ming GL. 2023. Development and Application of Brain Region–Specific Organoids for Investigating Psychiatric Disorders. *Biol Psychiatry* **93**:594–605. doi:10.1016/j.biopsych.2022.12.015

Figure Titles and Legends

Figure 1 Adherent cortical organoid model. A Schematic representation of the differentiation protocol. **B/C/D** Representative pictures of NPCs from three different iPSC lines with markers SOX2, Nestin and FOXG1 (scale bar B, 50 µm; C/D, 20 µm). **E** Live/Dead stain of a representative time course showing self-organization during differentiation, starting with radial organization between day 28 and day 42, seeding density 1500 NPCs per well; scale bars left to right 100 µm, 150 µm, 100 µm, 100 µm). **F** Full well showing radial organization at day 42 in culture were only a few dead cells are visible in red in the dense centre of the structure, seeding density 1500 NPCs per well (scale bar, 500 µm).

Figure 2 Adherent cortical organoids show an organized network of neuronal and astrocyte subtypes. A MAP2+ somas and dendrites alongside Tau+/MAP2- axons show segregation of dendritic and axonal compartments, with SOX2+ progenitors concentrated in the center of the organoid (Day 75, 200µm). **B** MAP2+ and NeuN+ cells indicate mature neurons (Day 72, 50 µm). **C** Deep-layer cortical marker CTIP2 and upper layer marker CUX1 show rudimentary segregation of cortical layers in expected inside-out pattern (Day 64, 50 µm). **D** Rudimentary separation of SOX2+ NPCs, CTIP2+ deep layer neurons and CUX1+ upper layer neurons (Day 67, scale bar 100 µm) **E** Full well overview of the CUX1 and CUX2 positive regions**.** **F** GAD67+ interneuron (white arrows) proportion of NeuN+ neurons (Day 67, 50 µm). **G** Quantification of GAD67+ proportion of NeuN+ neurons. Every point is the percentage of GAD67+ interneurons out of all NeuN+ neurons in a spatially randomized selected image with on average 130.6 (± 16.1) NeuN+ nuclei per frame. (Line 1: N= 26 images of 6 different cortical organoids at day 65-67; Line 2/3: 6 images of 2 different organoids at day 65). **H** Quantification of GAD67+ proportion of NeuN+ neurons of cell line

1, at 3 different time points. The number of GAD67+ interneurons over the total NeuN+ population remains relatively stable although at day 114 there was a modest increase which disappeared at day 242. Data was collected from 4-6 organoids per time point. **G/H** The different symbols reflect from which organoid the data point was collected**. I** Astrocyte markers GFAP and S100β show the general radial pattern of astrocyte outgrowth (Day 66, 500 µm). **J/K/L** GFAP staining reveals the morphologies of different astrocyte subtypes (white arrows), including fibrous astrocytes (**J**, Day 65, 100 µm), protoplasmic astrocytes (**K**, Day 65, 50 µm) and interlaminar astrocytes (**L**, Day 65, 100 µm). **M** Co-localization of astrocyte marker GFAP and PAX6 marks radial glia (white arrows) (Day 65, 50 µm).

Figure 3 Adherent cortical organoids form oligodendrocyte lineage cells. A Adherent cortical organoids show OPCs as early as 44 days, indicated by OPC marker NG2 (Day 44, 20 µm). **B/C** The NG2+ OPCs are still present in the cortical organoids after 4 months (Day 119, B 50 µm, C 20 µm). **D** Young oligodendrocytes start to emerge after 4 months indicated by rudimentary MBP staining (Day 119 100 µm and 20 µm). **E/F** After 5 months, MBP-positive oligodendrocytes show more mature morphology and initial wrapping of NF200+ axons (Day 148; E, 50 µm and 20 µm, F 5 µm). **G/H/I** Oligodendrocyte distribution at day 161 where the MBP+ oligodendrocytes sit between axons bundles and co-localize with NF200+ axons (G/H/I Day 161, G 500 µm, H 100µm, I 10 µm).

Figure 4 Adherent cortical organoids show a neural network with excitatory and inhibitory synapses. A Synapsin staining shows synapse formation along MAP2+ dendrites (Day 70, 20 µm). **B** Co-localization of pre-synaptic marker Synapsin and post-synaptic marker PSD-95 (Day 205, 20 µm). **C** MAP2+ dendrites and soma are decorated with Synapsin+ synapses

(Day 251, 100 µm) **D** Overview of entire well, showing alignment of Synapsin staining with MAP2 (Day 251, 500 µm)**. E** Sparse labeling of neurons with AAV9.CamKII.eGFP allows detailed imaging of glutamatergic dendritic spines with mature mushroom morphology, contacting pre-synaptic Synapsin puncta (Day 310, 5 µm). **F** Excitatory synapses marked by overlapping Synapsin+ and HOMER1+ puncta (scale bar: top 20 µm, bottom 5 µm). **G** Inhibitory synapses marked by overlapping Synapsin+ and Gephyrin+ puncta (scale bar: top 20 µm, bottom 5 µm). **H** Density of excitatory and inhibitory synapses per 100µm^2. There are about twice as much excitatory synapses (10.9 / 100 µm^2) as inhibitory synapses (5.0 / 100 µm^2). **I** The proportion of Synapsin that co-localizes with HOMER1 is 0.51 and the proportion of Synapsin that co-localizes with Gephyrin is 0.21.

Figure 5 Activity in the Adherent Cortical Organoids

A Snapshot of radially organized neurons transduced with AAV1.Syn.GCaMP6s.WPRE.SV40 (Day 60, 100 µm). **B** Representative calcium traces from active neurons in two different Fields of View (FOVs) from cell line 1, showing both individual activity and network bursts where each line corresponds to a single cell. **C** Events per minute of all recorded cells in day 61 and **100** (day 61, 3.9 ± 0.5 events/min; day 100, 3.9 ± 0.6 events/min). **D** Network bursts per minute (D61, average of 1.4 ± 0.07 NB/min; D100 average of 1.6 ± 0.12 NB/min) which shows all active cells are participating with the network bursts to some degree. **E** Percentage of events that are part of network bursts, which indicates that some cells only have events that are part of a network burst while for other cells the network bursts are only a small part of their total calcium events. The data was collected from 2-3 organoids per time point from 2 different batches of differentiation.

Supplementary Figure 1 Reproducibility of Neural Progenitor Cells and Adherent Cortical Organoids. A NPCs are positive for SOX2, Nestin, FOXG1, PAX6 and TBR2 (scale bars 20 μm) **B** LIVE/DEAD staining of adherent organoids (N=4) showing reproducibility of the structure formation. Seeding density line 1; 1250 NPCs, line 2; 750 NPCs, line 3; 1000 NPCs (scale bars 500 μm). **C** Proportion of properly formed single structure adherent cortical organoids. Each dot represents the end point of a different batch of adherent cortical organoids where the size of the batch ranges from 10-40 organoids per plate. Total organoids line 1 n=248, line 2 n=70, line 3 n=70. **D** Function of the necessary NPC seeding density to form adherent cortical organoids in relation to the doubling time as a measure of the proliferation rate of the NPCs. The doubling time of the NPCs explains more than half the variation (r^2 = 0.67) of the required seeding density showing that fewer cells need to be seeded for NPC lines with a higher proliferation rate.

Supplementary Figure 2 Neuronal maturation in cortical organoids is shown by a temporal shift in NPC and neuronal markers. A Representative images exhibiting change in expression of NPC and neuronal markers over time. Number of cells positive for NPC markers SOX2 and PAX6 decreases over time. Deep-layer CTIP2+ neurons start appearing at day 28, while upper-layer CUX1+ positive neurons appear in higher numbers around day 56. (Scale bars 20 μm). **B** The percentages of DAPI+ cells expressing each of the markers were quantified at four time points. Significant differences between week 2 and week 8 expression were seen for SOX2+ (down by 39.6 %), CTIP2+ (up by 13.5 %) and CUX1+ cells (up by 23.1 %). *** $p < 0.0001$, ANOVA one-way followed by Tukey- Kramer's multiple

correction test. Error bars indicate SEM, n=3-6 images taken over two wells, for each time point.

Supplementary Figure S3 Distribution of axons and dendrites in adherent cortical organoids Radially organized MAP2+/Tau+ dendrites along with both radially and circumferentially organized NF200+/Tau+ axons in duplicate for each cell line (Day 63, scale bars 500 µm)

Supplementary Figure S4 Cortical layering in the adherent cortical organoids A,B Separation of CUX1 and CUX2 expression (A day 70, scale bar 100 µm; B day 67, scale bar 500 µm) **C** A SOX2+ band/layer is visible in the centre of the ACO (day 63, scale bar 500 µm)

Supplementary Figure S5 Astrocyte distribution within Adherent Cortical Organoids The abundantly present GFAP+ and S100B+ astrocytes have a comparable distribution with the MAP2+ neurons in the ACOs. The astrocytes show radial patterns with many somas located in the centre as well as a large presence outside the centre (Day 63, scale bars 500 µm).

Figure 5 – Video 1

Video showing 10 minutes of calcium imaging of an ACO at Day 61 using the genetically encoded calcium indicator AAV1.Syn.GCaMP6s.WPRE.SV40 (rainbow filter indicates increasing calcium signal ranging from blue to red, speed increase indicated by time stamp in top left corner).

Figure 1

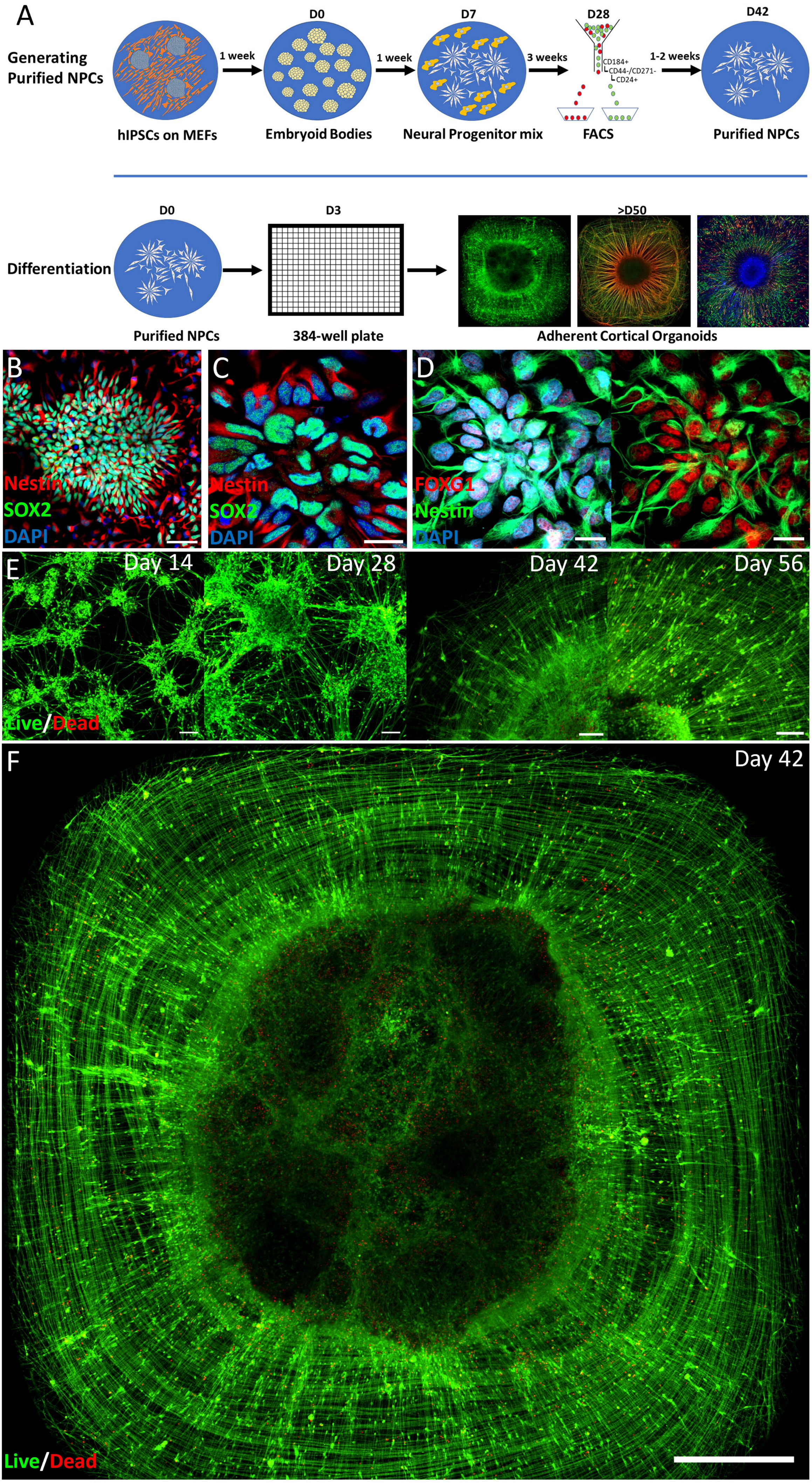
A
Generating Purified NPCs
D0
D7
D28
D42
1 week
1 week
3 weeks
1-2 weeks
CD184+
CD44-/CD271-
CD24+
hIPSCs on MEFs
Embryoid Bodies
Neural Progenitor mix
FACS
Purified NPCs
Differentiation
D0
D3
>D50
Purified NPCs
384-well plate
Adherent Cortical Organoids
B
Nestin
SOX2
DAPI
C
Nestin
SOX2
DAPI
D
FOXG1
Nestin
DAPI
E
Day 14
Day 28
Day 42
Day 56
Live/Dead
F
Day 42
Live/Dead

Figure 2

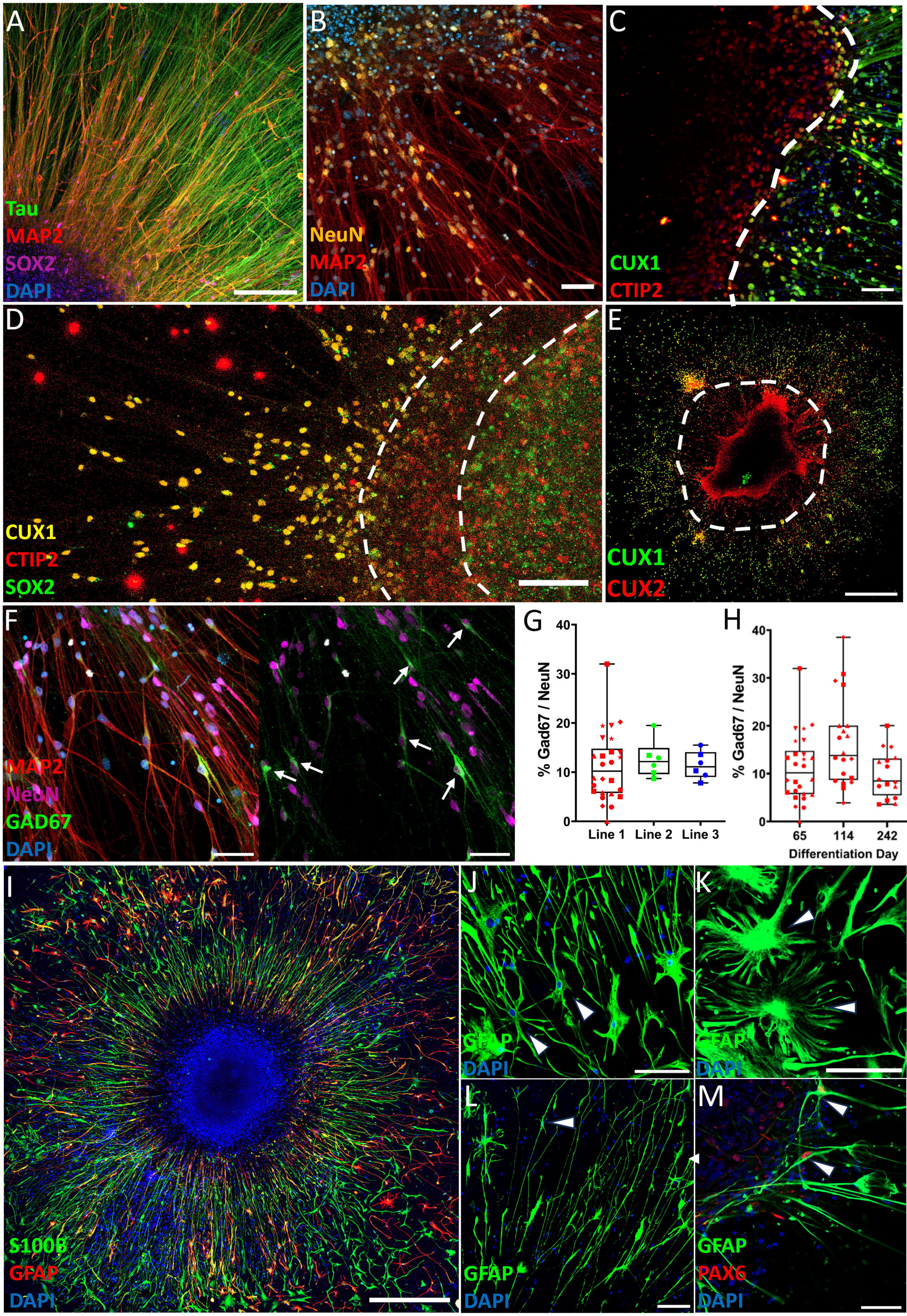
A
Tau
MAP2
SOX2
DAPI
B
NeuN
MAP2
DAPI
C
CUX1
CTIP2
D
CUX1
CTIP2
SOX2
E
CUX1
CUX2
F
MAP2
NeuN
GAD67
DAPI
G
% Gad67 / NeuN
0
10
20
30
40
Line 1
Line 2
Line 3
H
% Gad67 / NeuN
0
10
20
30
40
65
114
242
Differentiation Day
I
S100B
GFAP
DAPI
J
GFAP
DAPI
K
GFAP
DAPI
L
GFAP
DAPI
M
GFAP
PAX6
DAPI

Figure 3

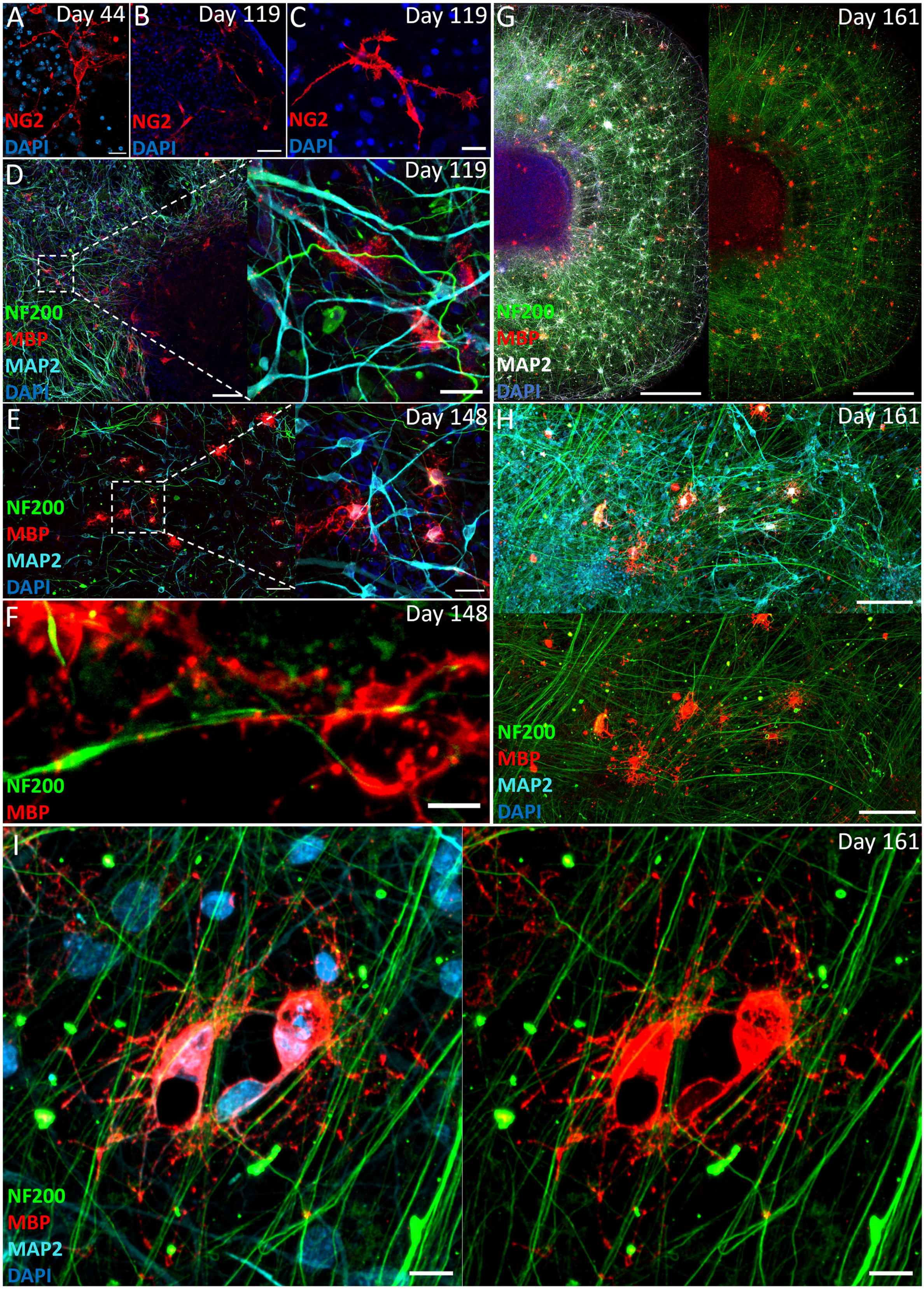
A
Day 44
NG2
DAPI
B
Day 119
NG2
DAPI
C
Day 119
NG2
DAPI
D
Day 119
NF200
MBP
MAP2
DAPI
E
Day 148
NF200
MBP
MAP2
DAPI
F
Day 148
NF200
MBP
G
Day 161
NF200
MBP
MAP2
DAPI
H
Day 161
NF200
MBP
MAP2
DAPI
I
Day 161
NF200
MBP
MAP2
DAPI

Figure 4

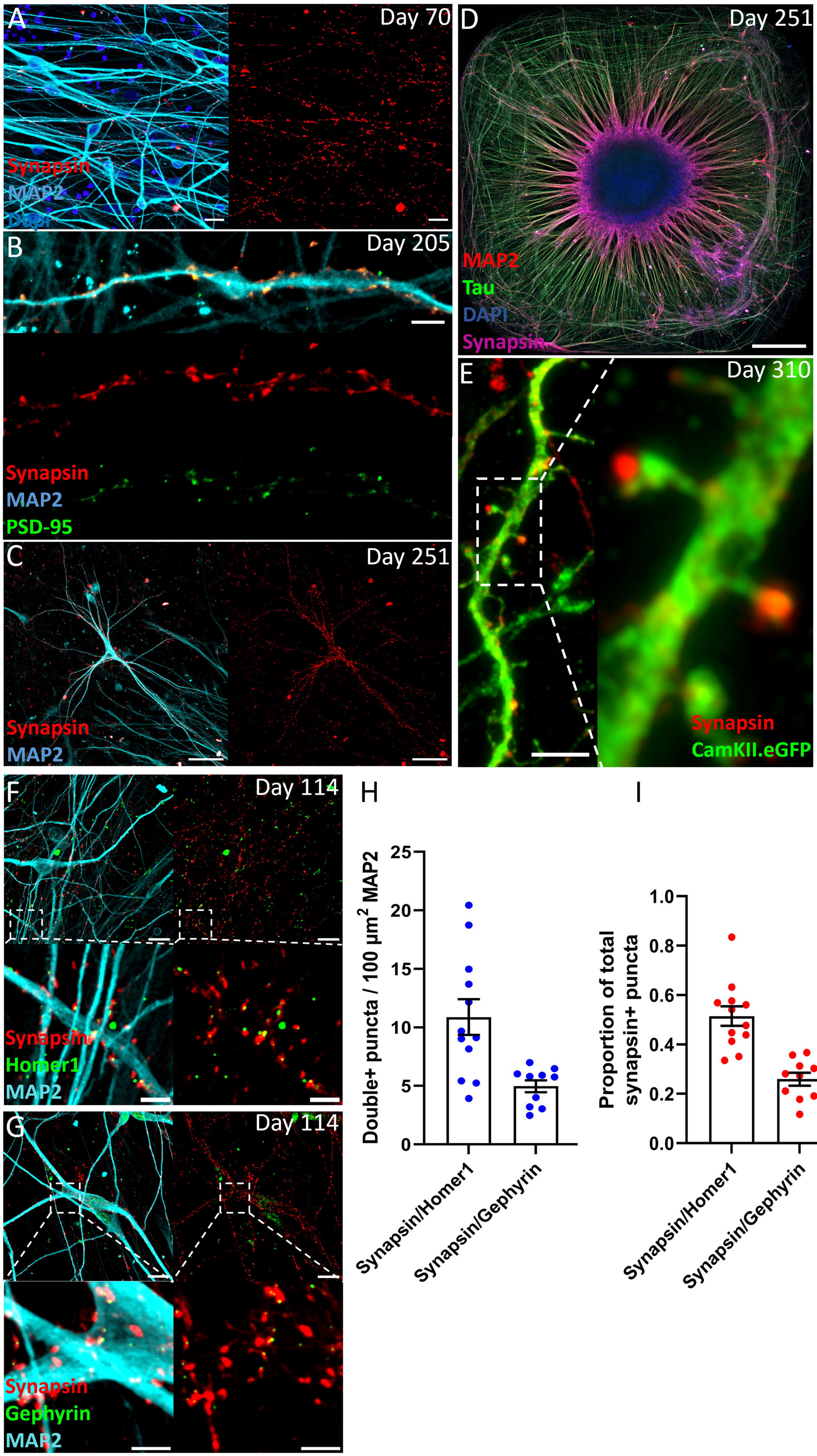
A
Day 70
Synapsin
MAP2
DAPI
B
Day 205
Synapsin
MAP2
PSD-95
C
Day 251
Synapsin
MAP2
D
Day 251
MAP2
Tau
DAPI
Synapsin
E
Day 310
Synapsin
CamKII.eGFP
F
Day 114
Synapsin
Homer1
MAP2
G
Day 114
Synapsin
Gephyrin
MAP2
H
Double+ puncta / 100 µm² MAP2
25
20
15
10
5
0
Synapsin/Homer1
Synapsin/Gephyrin
I
Proportion of total synapsin+ puncta
1.0
0.8
0.6
0.4
0.2
0.0
Synapsin/Homer1
Synapsin/Gephyrin

Figure 5

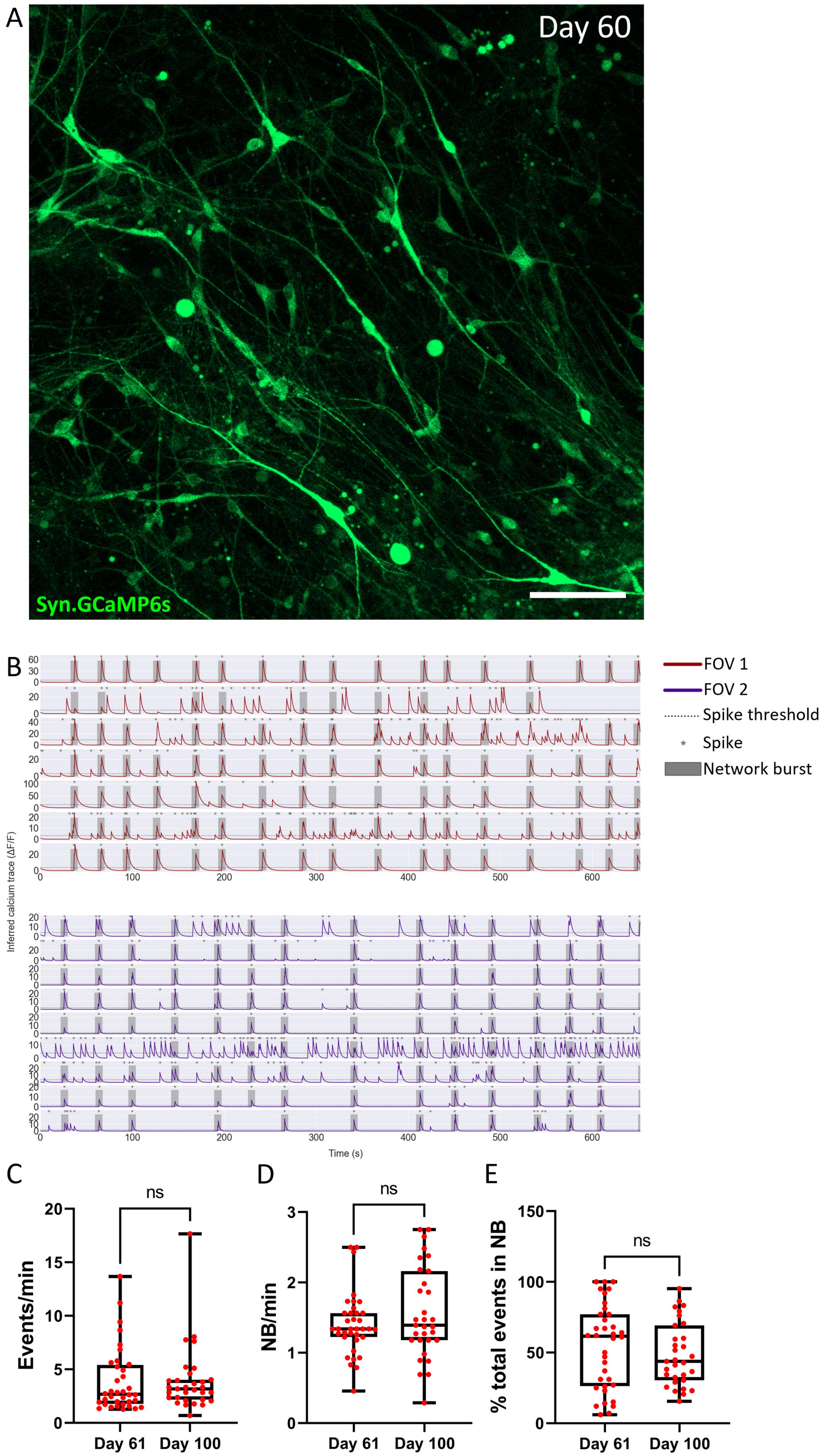
A
Day 60
Syn.GCaMP6s
B
FOV 1
FOV 2
Spike threshold
Spike
Network burst
Inferred calcium trace (ΔF/F)
Time (s)
C
ns
Events/min
Day 61
Day 100
D
ns
NB/min
Day 61
Day 100
E
ns
% total events in NB
Day 61
Day 100